Inorganica Chimica Acta 390 (2012) 135–142

Contents lists available at SciVerse ScienceDirect

Inorganica Chimica Acta

journal homepage: www.elsevier.com/locate/ica

Construction and property investigation of inorganic–organic hybrid materials based on metal–salens and Keggin polyoxometalates

Xing Meng, Hai-Ning Wang, Xin-Long Wang *, Guang-Sheng Yang, Shuang Wang, Kui-Zhan Shao, Zhong-Min Su *

Institute of Functional Material Chemistry, Key Lab of Polyoxometalate Science of Ministry of Education, Faculty of Chemistry, Northeast Normal University, Changchun 130024, People's Republic of China

ARTICLE INFO

Article history:
Received 30 December 2011
Received in revised form 28 March 2012
Accepted 4 April 2012
Available online 13 April 2012

Keywords:
Hybrid materials
Keggin polyanion
Metal–salens
Photocatalytic activity
Electrochemical behaviors

ABSTRACT

Four hybrid materials based on the Keggin polyanions and metal–salens, namely, $[Mn(salen)(CH_3OH)_2]_4[SiW_{12}O_{40}]$ (**1**), $[Mn(salen)(H_2O)]_2[Mn(salen)(H_2O)][PW_{12}O_{40}]$ (**2**), $[NH(CH_2CH_3)_3]_2[Mn(salen)(CH_3OH)]_2[SiW_{12}O_{40}]\cdot 2CH_3OH$ (**3**), and $[(Cu(salen))_2Cu(H_2O)]_2[SiW_{12}O_{40}]$ (**4**) (H_2salen = N,N′-ethylenebis(salicylideneimine)) have been successfully synthesized. All the compounds are characterized by X-ray single-crystal diffractions, elemental analyses, IR spectra, and thermogravimetric analyses (TGA). Crystal structure analysis reveals that compound **1** exhibits a supramolecular structure containing one Keggin-type $[SiW_{12}O_{40}]^{4-}$ heteropolyanion and four Mn^{III}–salen units. In compound **2**, the $[PW_{12}O_{40}]^{3-}$ polyoxoanions and Mn^{III}–salen complex cations are regularly arranged along the *c*-axis showing an alternating packing arrangement of anionic and cationic layers. While in compound **3**, the polyoxoanion $[SiW_{12}O_{40}]^{4-}$ is covalently decorated by two $[Mn(salen)(CH_3OH)]^+$ fragments via two terminal oxygen atoms in the opposite sites, giving birth to an unusual Keggin anion supporting transition metal–salen complexes. Compound **4** represents the first example that POM supports trinuclear copper–salen complexes. Photocatalytic experiments of **1**–**4** indicate that they possess high catalytic activity for photodegradation of RhB under UV irradiation. In addition, the electrochemical behaviors of **1** and **2** are well investigated.

1. Introduction

Polyoxometalates (POMs) exhibit a wide variety of properties such as catalysis [1], magnetism [2], electrochemistry [3] and photochromism [4] and represent an emerging material [5] with respect to their potential applications in various fields [6]. Hybrid inorganic–organic materials based on POMs attract more and more interest owing to their considerable structural versatility related with their sizes and functions. In these compounds, transition-metal fragments combine with POMs forming either discrete units or multi-dimensional structures through providing charge compensation [7], or coordinating to terminal oxo groups [8]. In this aspect, the modification of POMs via electrostatic force interactions to polyanions or covalent linking of transition-metal complexes is very important because it can fine-tune their properties [9].

The synthesis of functional inorganic–organic hybrid architectures, which can maintain their original nature and simultaneously form novel synergetic interactions between inorganic clusters and organic/metal–organic building units, has been extensively developed in recent years. Generally, there are two synthetic strategies to prepare hybrid POMs. One strategy is that organic species act as structure-directing components of inorganic–organic hybrids to decorate polyoxoanions; the other is to modify the polyoxoanions with transition-metal complexes: the metal ion bridges the inorganic clusters and organic ligands. Most of hybrid POMs based on the two strategies generated by means of 'one pot' reaction. This synthetic approach cannot predict the final structure definitely due to the unclear formation mechanism and various coordination numbers of metal ions. Therefore, we adopt a 'complex ligand' strategy [10] to construct inorganic–organic hybrids: transition-metal complexes are predetermined as the substrates and then involve in a subsequent process occurring between transition-metal complexes and POMs.

Among the various different types of POMs, we chose the Keggin heteropolyanions, as they were the most widely recognized and thoroughly studied. Furthermore, we used metal–salen for our synthetic strategy based on the following considerations: (i) it is noted that salen ligands prefer to adopting quasi-planar forms to coordinate with metal centers in the equatorial plane, thereby two residual longitudinal active sites make metal–salen complexes be an ideal coordination–acceptor to combine with different building units to construct various functional materials [11]; (ii) metal–salen has powerful applications in the fields of catalysis, magnetic

* Corresponding authors. Tel.: +86 431 85099108.
E-mail address: zmsu@nenu.edu.cn (Z.-M. Su).

0020-1693/$ - see front matter © 2012 Elsevier B.V. All rights reserved.
http://dx.doi.org/10.1016/j.ica.2012.04.011

materials, and bioinorganic chemistry [12]; (iii) limited efforts has been paid to combining metal–salen to construct organometallic–inorganic hybrid compounds so far [13], and further work is still necessary to proceed. Herein, we reported the syntheses and characterization of four POMs-based metal salen compounds, namely, $[Mn(salen)(CH_3OH)_2]_4[SiW_{12}O_{40}]$ (**1**) $[Mn(salen)(H_2O)]_2[Mn(salen)(H_2O)][PW_{12}O_{40}]$ (**2**) $[NH(CH_2CH_3)_3]_2[Mn(salen)(CH_3OH)]_2[SiW_{12}O_{40}]\cdot 2CH_3OH$ (**3**) and $[(Cu(salen))_2Cu(H_2O)]_2[SiW_{12}O_{40}]$ (**4**). The single-crystal X-ray diffraction, elemental analysis, IR spectra and TGA studies are performed on them. What's more, the photocatalytic activities of compounds **1**–**4** and the electrochemical behaviors of compounds **1** and **2** have been investigated in detail.

2. Experimental section

2.1. Materials and instruments

All starting materials and solvents were reagent grade, commercially available and used without further purification. $Mn(salen)(H_2O)_2ClO_4$ and $[Cu(salen)]_2Cu(H_2O)_2(ClO_4)_2$ were synthesized according to the reported procedures [14]. The Fourier transform infrared (FT-IR) spectra were recorded in the range 4000–400 cm^{-1} on a Mattson Alpha-Centauri spectrometer with pressed KBr pellets. Elemental analyses (C, H, and N) were carried out on a Perkin–Elmer 240C elemental analyzer. TG analyses were performed on a Perkin–Elmer TG-7 analyzer heated from room temperature to 900 °C under a N_2 atmosphere at a rate of 10 °C min^{-1}. All electrochemical measurements were carried out on a CHI 600B electrochemical workstation at room temperature (25–30 °C). The working electrodes were prepared as the literature reported method [15]. Chemically bulk-modified carbon paste electrodes (CPEs) were used as working electrodes. An Ag/AgCl electrode was used as reference electrode and platinum wire was used as a counter electrode.

2.1.1. Photocatalysis experiments

The aqueous solution was prepared by addition of the sample (1.0×10^{-5} mol compounds) to a 50 mL rhodamine-B (RhB) solution (2.0×10^{-5} M) at pH 3.5 which was adjusted with dilute aqueous solution of either $HClO_4$ or NaOH. The solution was stirred with a magnetic stir and exposed to UV irradiation from a 125 W Hg lamp at a distance of 3–4 cm between the liquid surface and the lamp. The solution was still stirred during irradiation. At given time intervals, approximately 1.0 ml of sample was taken out of the beaker for UV–Vis absorption spectrum analysis.

2.2. Synthesis

Caution! Perchlorates are potentially explosive and should be treated in small quantities with care.

2.2.1. Synthesis of $Mn(salen)(H_2O)_2ClO_4$

A mixture of an ethanol solution (15 cm^3) of ethylenediamine (0.06 g, 1 mmol) and 0.244 g (2 mmol) of salicylaldehyde in 15 cm^3 of ethanol was stirred for 2 h, with subsequent addition of ethanol (20 cm^3) of $Mn(ClO_4)_2\cdot 6H_2O$ (0.362 g, 1 mmol). The resulting solution was stirred for 10 min, and then 0.10 g (1 mmol) of triethylamine added. A deep-brown solution was obtained, which was refluxed for 2 h, then allowed to stand at room temperature.

2.2.2. Synthesis of $[Cu(salen)]_2Cu(H_2O)_2(ClO_4)_2$

$[Cu(salen)]_2Cu(H_2O)_2(ClO_4)_2$ was prepared in the same way as compound $Mn(salen)(H_2O)_2ClO_4$ but using $Cu(ClO_4)_2\cdot 6H_2O$ (0.3705 g, 1 mmol) instead of $Mn(ClO_4)_2\cdot 6H_2O$ (0.362 g, 1 mmol).

2.2.3. Synthesis of $[Mn(salen)(CH_3OH)_2]_4[SiW_{12}O_{40}]$ (**1**)

$H_4[SiW_{12}O_{40}]$ (1.440 g, 0.5 mmol) was dissolved in 20 ml distilled water. Then, 20 ml $Mn(salen)(H_2O)_2ClO_4$ (0.913 g, 2 mmol) methanol solution was quickly added to above solution. The dark brown reaction mixture appeared immediately and was vigorous stirred in a rockered flask at 35 °C for 2 days. After filtration, the precipitate was recrystalled from CH_2Cl_2 and CH_3OH (1:1) solution. Dark-brown plate-like crystals of **1** were obtained in 59% yield based on W. Elemental *Anal*. Calc. for $C_{72}H_{88}Mn_4N_8O_{56}SiW_{12}$ (4415.55): C, 19.58; H, 2.01; N, 2.54. Found: C, 19.34; H, 2.16; N, 2.76%. IR (cm^{-1}): 797.31(s) 920.19(s) 1619.75(m) 466.81(m) 524.45(m) 632.36(m) 967.69(m) 1541.51(m) 1283.60(w) 1443.20(w) 1015.14(w) 1127.97(w) 1207.61(w) 1390.06(w) 3423.19(w).

2.2.4. Synthesis of $[Mn(salen)(H_2O)]_2[Mn(salen)(H_2O)][PW_{12}O_{40}]$ (**2**)

$H_3[PW_{12}O_{40}]$ (1.440 g, 0.5 mmol) was dissolved in 20 ml distilled water. Then, 20 ml $Mn(salen)(H_2O)_2ClO_4$ (0.456 g, 1 mmol) methanol solution was quickly added to above solution. The dark brown reaction mixture appeared immediately and was vigorous stirred in a rockered flask at 35 °C for 2 days. After filtration, the precipitate was recrystalled from acetonitrile solution. Dark-brown plate-like crystals of **2** were obtained in 64% yield based on W. Elemental *Anal*. Calc. for $C_{48}H_{48}Mn_3N_6O_{49}PW_{12}$ (3894.91): C, 14.80; H, 1.24; N, 2.16. Found: C, 14.57; H, 1.49; N, 2.31%. IR (cm^{-1}): 811.10(s) 978.73(s) 1078.90(m) 895.34(m) 514.68(m) 467.20(m) 628.95(m) 593.20(m) 1604.78(m) 1289.29(m) 1443.74 (w) 1544.08(w) 3441.06(w) 1390.90(w).

2.2.5. Synthesis of $[NH(CH_2CH_3)_3]_2[Mn(salen)(CH_3OH)]_2[SiW_{12}O_{40}]\cdot 2CH_3OH$ (**3**)

$H_4[SiW_{12}O_{40}]$ (1.440 g, 0.5 mmol) was dissolved in 20 ml distilled water. Then, 20 ml $Mn(salen)(H_2O)_2ClO_4$ (0.913 g, 2 mmol) methanol solution was quickly added to above solution and two drops of triethylamine were also added. The dark brown reaction mixture appeared immediately and was vigorous stirred in a rockered flask at 35 °C for 2 days. After filtration, the precipitate drying at 70 °C and was recrystalled from CH_2Cl_2 and CH_3OH (1:1) solution. Dark-brown plate-like crystals of **3** were obtained in 54% yield based on W. Elemental Anal *Anal*. Calc. for $C_{48}H_{74}Mn_2N_6O_{52}SiW_{12}$ (3911.30): C, 14.74; H, 1.91; N, 2.15. Found: C, 14.57; H, 1.77; N, 2.39%. IR (cm^{-1}): 794.95(s) 919.63(s) 525.97(m) 465.53(m) 969.70(m) 1618.90(m) 1015.34(m) 1285.10(m) 1442.77(m) 1540.62(m) 1206.88(w) 1153.83(w) 1390.72(w) 1129.54(w) 1331.16(w) 3452.31(w) 3054.10(w).

2.2.6. Synthesis of $[(Cu(salen))_2Cu(H_2O)]_2[SiW_{12}O_{40}]$ (**4**)

The synthesis of **4** was similar to **1** except that $[Cu(salen)]_2Cu(H_2O)_2(ClO_4)_2$ was used instead of $Mn(salen)(H_2O)_2ClO_4$. Dark-brown plate-like crystals of **4** were obtained in 56% yield based on W. Elemental *Anal*. Calc. for $C_{64}H_{60}Cu_6N_8O_{50}SiW_{12}$ (4356.73): C, 17.64; H, 1.39; N, 2.57. Found: C, 17.47; H, 1.51; N, 2.39%. IR (cm^{-1}): 1628.46(s) 1446.36(s) 1531.88(s) 735.59(s) 1190.44(m) 1598.04(m) 1328.94(m) 1133.85(m) 1303.24(m) 1388.59(m) 1050.13(m) 851.56(m) 1084.19(m) 570.42(m) 975.87(w) 464.01(w) 901.12(w) 1025.57(w) 2953.22(w) 2916.05(w) 3016.08(w) 3049.77(w) 3422.35(w) 1235.74(w) 613.36(w) 928.12(w) 787.87(w) 438.14(w) 641.67(w) 497.73(w).

2.3. Synthsis discussion

Because of the low stability of Schiff-base ligands, water/solvent hydrothermal technology can not be used in this system. In the course of the synthesis, the main difficulty is to choose suitable solvent media. Most of the POMs are synthesized in aqueous solution and tend to form precipitation in organic solutions. While, most of the metal–salen compounds are isolated from methanol soluion.

Table 1
Crystal data and structure refinement for **1**–**4**.

Compound	**1**	**2**	**3**	**4**
Formula	$C_{72}H_{88}Mn_4N_8O_{56}SiW_{12}$	$C_{48}H_{48}Mn_3N_6O_{49}PW_{12}$	$C_{48}H_{74}Mn_2N_6O_{52}SiW_{12}$	$C_{64}H_{60}Cu_6N_8O_{50}SiW_{12}$
Formula weight	4415.55	3894.91	3911.30	4356.73
Space group	$P\bar{1}$	$P\bar{1}$	$P\bar{1}$	Pbca
Unit cell dimensions				
a (Å)	12.437(5)	15.378(5)	11.893(5)	14.939(5)
b (Å)	14.520(5)	15.993(5)	13.102(5)	23.406(5)
c (Å)	16.254(5)	18.636(5)	14.788(5)	34.243(5)
α (°)	107.875(5)	100.932(5)	68.768(5)	90.000(5)
β (°)	91.203(5)	103.704(5)	76.765(5)	90.000(5)
γ (°)	90.528(5)	101.332(5)	69.485(5)	90.000(5)
ρ (g cm^{-3})	2.626	3.058	3.251	2.417
V (Å^3)	2792.5(17)	4230(2)	1997.9(13)	11973(5)
Z	1	2	1	4
R_{int}	0.0335	0.0507	0.0360	0.1242
$F(000)$	2026	3496	1772	7904
Reflections collected/unique	13834/9660	21097/14656	10100/6926	58870/10859
Goodness-of-fit (GOF) on F^2	1.085	1.024	1.137	0.960
$R_1(I > 2\sigma(I))$[a]	0.0923	0.0563	0.0687	0.0692
wR_2[b]	0.2675	0.1743	0.1566	0.2084

[a] $R_1 = \Sigma||F_o| - |F_c||/\Sigma|F_o|$.
[b] $wR_2 = |\Sigma w(|F_o|^2 - |F_c|^2)|/\Sigma|w(F_o^2)^2|^{1/2}$.

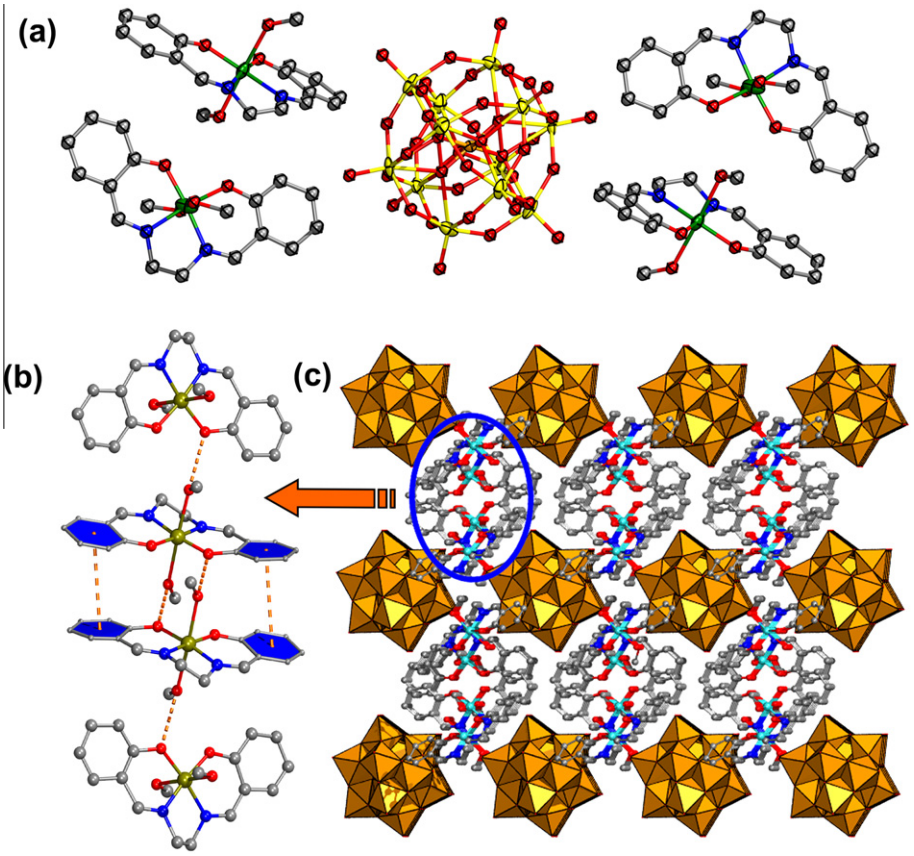

Fig. 1. (a) The molecular structure unit of compound **1**. (b) The hydrogen bonds and π–π stacking interactions between metal–salen cation segments. (c) The packing diagram of compound **1** along *b*-axis. All the hydrogen atoms have been omitted for clarity.

So the mixed methanol-water solution was adopted in the system. In addition, POMs can only maintain their structures in narrow pH range, and Schiff-base ligands are not stable in relatively high temperature. So choose suitable pH and the temperature are the key factors for the formation of the compounds.

2.4. Crystallography

X-ray diffraction data for compounds were collected on a Bruker Smart Apex-II CCD diffractometer using graphite-monochromated Mo Kα radiation (λ = 0.71073 Å) at room temperature. The four

crystal structures were solved by the direct method of SHELXS-97 [16] and refined with full-matrix least-squares techniques (SHELXL-97) [17] within WINGX [18]. All of the non-hydrogen atoms were refined anisotropically. The hydrogen atoms of organic ligands were fixed on calculated positions. Some H atoms of the ligand could not be introduced in the refinement but were included in the structure factor calculation. Further details of the crystallographic data and refinement parameters were given in Table 1.

3. Results and discussion

3.1. Structure description of compound **1**

Compound **1** crystallizes in the triclinic space group $P\bar{1}$). The basic structural unit of **1** contains four $[Mn(salen)(CH_3OH)_2]^+$ cation segments and one keggin-type $[SiW_{12}O_{40}]^{4-}$ heteropolyanion. As shown in Fig. 1a, the naked polyoxoanion $[SiW_{12}O_{40}]^{4-}$ is wholly enwrapped by the four $[Mn(salen)(CH_3OH)_2]^+$ moieties and connected with each other via the electrostatic attraction. The polyoxoanion $[SiW_{12}O_{40}]^{4-}$ is a typical Keggin structure with an approximate Td symmetry, which consists of a central $\{SiO_4\}$ tetrahedron surrounded by twelve $\{WO_6\}$ octahedra arranged in four groups of three edge-sharing octahedral units. Each of the trinuclear units is in turn linked by corner sharing to each other and to the central $\{SiO_4\}$ tetrahedron. In $[Mn(salen)(CH_3OH)_2]^+$ cation segments, six-coordinated Mn^{III} cations exhibit identical distorted octahedral configuration, coordinated by two nitrogen atoms and two oxygen atoms from one salen ligand at equatorial sites, two oxygen atoms from two methanol molecules at the polar sites. In the equatorial plane, the average bond length of Mn–O(N) is 1.91 Å. In the polar positions, the average Mn–O bond length is 2.30 Å. Elongated axial Mn–O bonds attributes to Jahn–Teller distortion at the high-spin d^4 metal center. All the Mn centers possess the +3 oxidation states based on the charge balance considerations [19], as well as the presence on Mn centers of a Jahn–Teller elongation axis.

Stabilization of the compound in the crystal lattice is increased via various intermolecular forces. In the metal–salen cation segments, hydrogen bonds (O46–H···O41 (distance of 2.68(2) Å) and O45–H···O43 (distance of 2.87(5) Å)) and π–π stacking interactions (face-to-face distance of ca. 3.61 Å) have been found, which make a closed packing cationic layer. These interactions are highlighted in Fig. 1b. In addition, the metal–salen cationic layer interact with the polyoxometalate anionic layer through electrostatic attraction and van der Waals forces. Thus, a three dimensional supramolecular assembly comes into being along the *b*-axis (Fig. 1c).

3.2. Structure description of compound **2**

Single-crystal X-ray diffraction analysis reveals that compound **2** crystallizes in the triclinic space group $P\bar{1}$. As shown in Fig. 2, the asymmetric unit of **2** consists of one $[Mn(salen)(H_2O)]_2^{2+}$ dimer, one $[Mn(salen)(H_2O)]^+$ cation fragment, and one $[PW_{12}O_{40}]^{3-}$ polyoxoanion. There are two kinds of Mn centers exhibiting distinct coordination geometries. In the $[Mn(salen)(H_2O)]_2^{2+}$ dimer (Fig. S5a in the ESI†), Mn^{III} ions are six-coordinated and possess distorted octahedral configurations, coordinated by two nitrogen atoms and two oxygen atoms from one salen ligand in the equatorial positions with an average Mn–N(O) distance of 1.923 Å, one oxygen atom from the other salen ligand and one oxygen atom from water molecule in the axial sites (average distance of 2.332 Å). The intra-core Mn···Mn distance is 3.334(4) Å, while the Mn(1)–O(43)–Mn(2) and Mn(2)–O(44)–Mn(1) angles are 99.1(5)° and 99.3(6)°, respectively. In the $[Mn(salen)(H_2O)]^+$ fragment (Fig. S5b in the ESI†), five-coordinated Mn^{III} center shows a distorted square-pyramidal coordination environment, bonded by two nitrogen atoms and two oxygen atoms from a salen ligand in the equatorial positions with an average Mn–N(O) distance of 1.903 Å, one oxygen atom from one water molecule in the axial position.

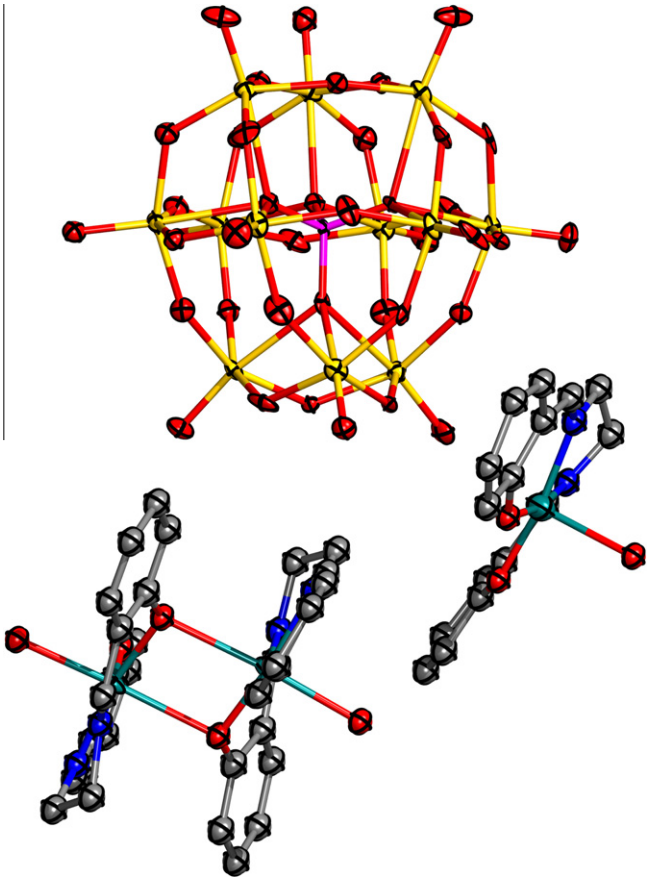

Fig. 2. The molecular structure unit of compound **2**. All the hydrogen atoms have been omitted for clarity.

In the unit cell of compound **2**, the metal-organic donors and inorganic polyoxoanions are regularly arranged along *c*-axis. The whole structure can be described as the packing of anionic and cationic layers along the *c*-axis as shown in Fig. 3. The cationic layer is formed by $[Mn(salen)(H_2O)]^+$ fragments and $[Mn(salen)(H_2O)]_2^{2+}$ dimers. The anionic layer is constructed by isolated $[PW_{12}O_{40}]^{3-}$ polyoxoanions. The distance between the cationic layer and the anionic layer may be too far to exist hydrogen bonds. So the cohesion between the two layers is carried out by electrostatic forces and van der Waals forces. Two successive layers are parallel to each other. So, the whole packing arrangement of **2** can be view as an "ABAB" style by the simplified diagram (Fig. 3(right)). Notably, free void space is also present within the structure (16% of the crystal volume as calculated by PLATON).

3.3. Structure description of compound **3**

Compound **3** crystallizes in the triclinic space group $P\bar{1}$). The basic structural unit of **3** is shown in Fig. 4a, there are one $\{[Mn(salen)(CH_3OH)]_2[SiW_{12}O_{40}]\}^{2-}$ anion segment, two $NH(CH_2CH_3)^+$ cations and two solvent menthol molecules. Protonated triethylamine molecules act as the counterions and contact with adjacent $\{[Mn(salen)(CH_3OH)_2][SiW_{12}O_{40}]^{4-}\}^{2-}$ anionic subunits by the electrostatic force. The$\{[Mn(salen)(CH_3OH)]_2$

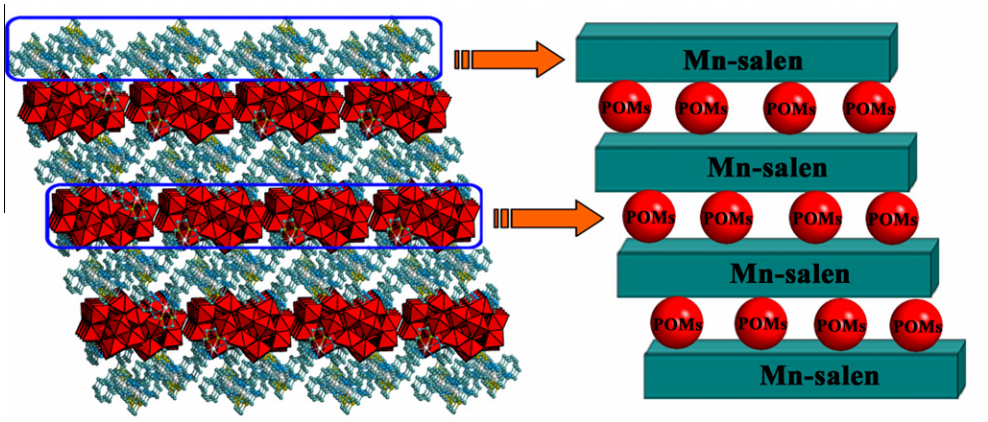

Fig. 3. The packing diagram of compound **2** along *c*-axis (left) and schematic illustration of the alternating packing arrangement of anionic and cationic layers (right). All the hydrogen atoms have been omitted for clarity.

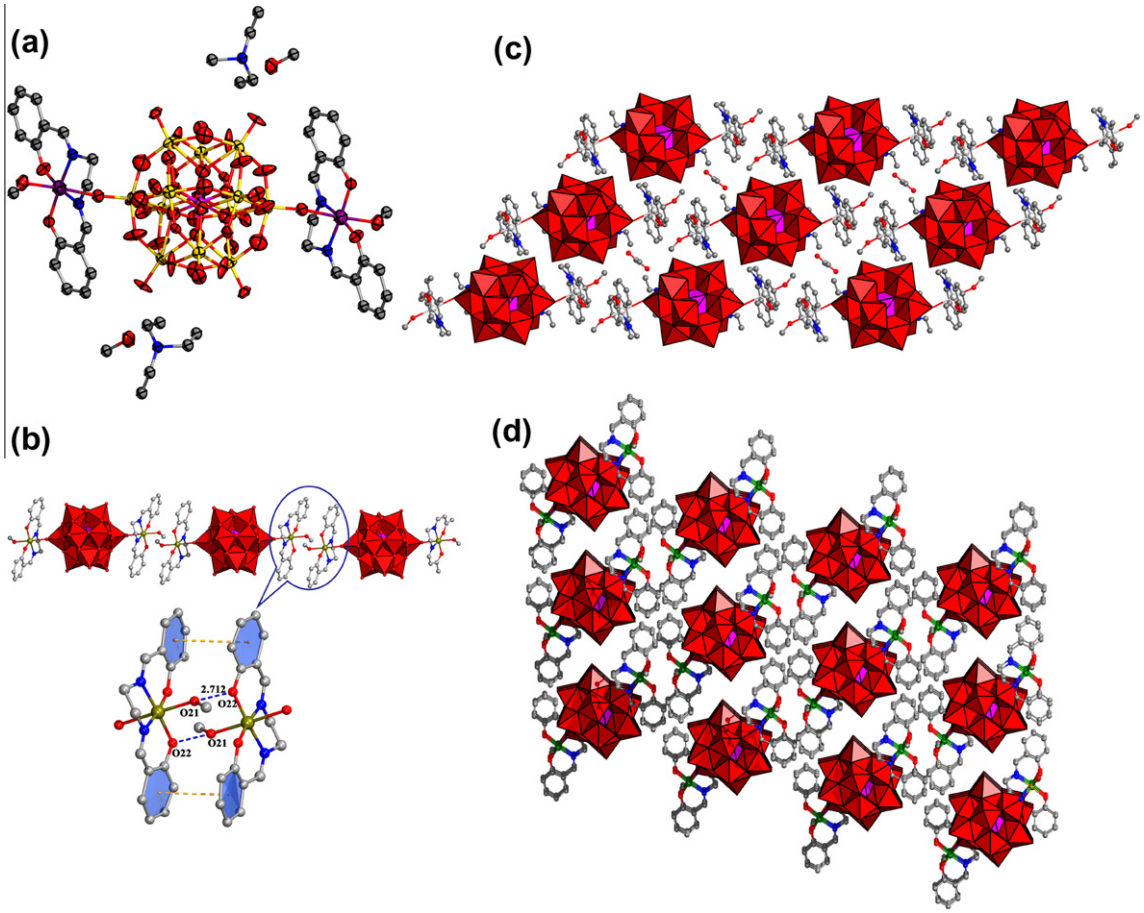

Fig. 4. (a) The molecular structure unit of compound **3**. (b) The 1D chain of compound **3**. (c) The two dimensional supramolecular layer of compound **3**. (d) The packing diagram of compound **3** along *a*-axis. All the hydrogen atoms have been omitted for clarity.

$[SiW_{12}O_{40}]\}^{2-}$ polyoxoanion is constructed from a $[SiW_{12}O_{40}]^{4-}$ cluster decorated by two $[Mn(salen)(CH_3OH)]^{+}$ units. The $[SiW_{12}O_{40}]^{4-}$ polyanion is a distorted α-Keggin structure. The central Si1 atom is surrounded by a distorted cube constituted of eight oxygen atoms with each oxygen site half-occupied. This structure feature often appears in the Keggin structure [20]. One of outstanding structural features is that each $[SiW_{12}O_{40}]^{4-}$ unit forms a covalent interaction with two $[Mn(salen)(CH_3OH)]^{+}$ fragments via the terminal oxygen atoms of the $[SiW_{12}O_{40}]^{4-}$ anion in the opposite sites with Mn-O distance of 2.346(16) Å. The Mn centers are in an axially elongated octahedral geometry, in which two nitrogen atoms and two oxygen atoms from one salen ligand are located at the equatorial positions with an average Mn–N(O) distance of 1.941 Å, while the axis sites are occupied by one oxygen atom from a methanol molecule and one oxygen atom deriving from the Keggin-type polyanion. In the axial positions, the average Mn–O bond length is 2.279 Å, which is slightly longer due to Jahn–Teller distortion at the high-spin d^4 metal center.

It is noteworthy that the $\{[Mn(salen)(CH_3OH)]_2[SiW_{12}O_{40}]\}^{2-}$ unit is just like a butterfly, where $[Mn(salen)(CH_3OH)_2]^+$ moieties appending to the periphery of POMs is the wings. All the wings are stacked in a staggered mode. Based on this model, these units can firstly extend into 1D chains via strong O21–H···O22 hydrogen bond (distance of 2.712 Å) and π–π stacking interactions between aromatic rings (face-to-face distance of ca. 3.49 Å) (Fig. 4b). Interestingly, oxygen atoms (O6 and O20) from the POMs involve in hydrogen bond interactions between Mn–salen units and the POMs, where carbon atoms from Mn–salen act as donors and oxygen atom of POMs as acceptors. By means of C7–H···O20 hydrogen bond (distance of 3.12(3) Å), a 2D supramolecular sheet generates (Fig. 4c). With the aid of C9–H···O6 (distance of 3.00(3) (Å)) hydrogen bond interaction, the layers parallel stack along *a* direction, and naturally a 3D supramolecular architecture comes into being (Fig. 4d).

Compared with the structures that have been synthesized [13], compound **3** is remarkable in that: (i) Compound **3** is the first example that the Keggin anion supports transition metal–salen complexes. (ii) In the process of self-assembly to form 1D supramolecular chain, there exist two kinds of electrostatic forces. (iii) In the 12 terminal oxygen atoms of the POM, two oxygen atoms take part in the coordination and four in the opposite positions involve in the hydrogen bond interactions leading to the generation of 3D supramolecular architecture.

3.4. Structure description of compound *4*

Compound **4** crystallizes in the orthorhombic space group *Pbca*. As shown in Fig. 5a, The basic structural unit $[(Cu(salen))_2Cu(H_2O)]_2[SiW_{12}O_{40}]$ is constructed from a $[SiW_{12}O_{40}]^{4-}$ cluster decorated by two $[(Cu(salen))_2Cu(H_2O)]^+$ units. An unusual feature in **4** is that there are two types of copper centers. Both Cu(1) and Cu(2) ions exhibit identical distorted square planar coordination environment, and are coordinated by two oxygen atoms and two nitrogen atoms from one salen ligand with an average Cu–N(O) distance of 1.92 Å. While Cu(3) ion possesses a distinct environment, which is six-coordinated, and shows a distorted octahedral sphere coordinated by one oxygen atom of the water molecule, and a terminal oxygen atom from the POM in addition to four oxygen atoms shared by Cu(1) and Cu(2). The average Cu–O distance is 2.321 Å. With the aid of bridge oxygen atoms, a trinuclear copper cluster generates which contains different Cu ions adopting distinct coordination modes.

The most prominent structural feature of **4** is that two $[(Cu(salen))_2Cu(H_2O)]^+$ subunits are covalently bonded to the polyoxoanion $[SiW_{12}O_{40}]^{4-}$ in the opposite directions, thus a Keggin anion supporting trinuclear copper–salen complexes form. Obviously, each unit enclosed by six others aggregates together through π–π interactions existing in Cu–salen (face-to-face distance of ca. 3.40 Å and face-to-face distance of ca. 3.46 Å) making up a 2D wave layer structure (Fig. 5b). As shown in Fig. 5c, the distance between the two layers is likely too far to exist hydrogen bonds. So the cohesion between the two layers is carried out by van der Waals forces. To the best of our knowledge, this compound represents the first example in which POM supports trinuclear copper–salen complexes.

There are some similar structural features between **3** and **4**: (i) Both possess butterfly-shape structures. (ii) The Keggin anion supports two transition metal complexes in the opposite directions. Subtle differences are also observed: (i) The transition metal in **4** shows two types of coordination modes. (ii) A trinuclear copper cluster exists in **4** which is uncommon.

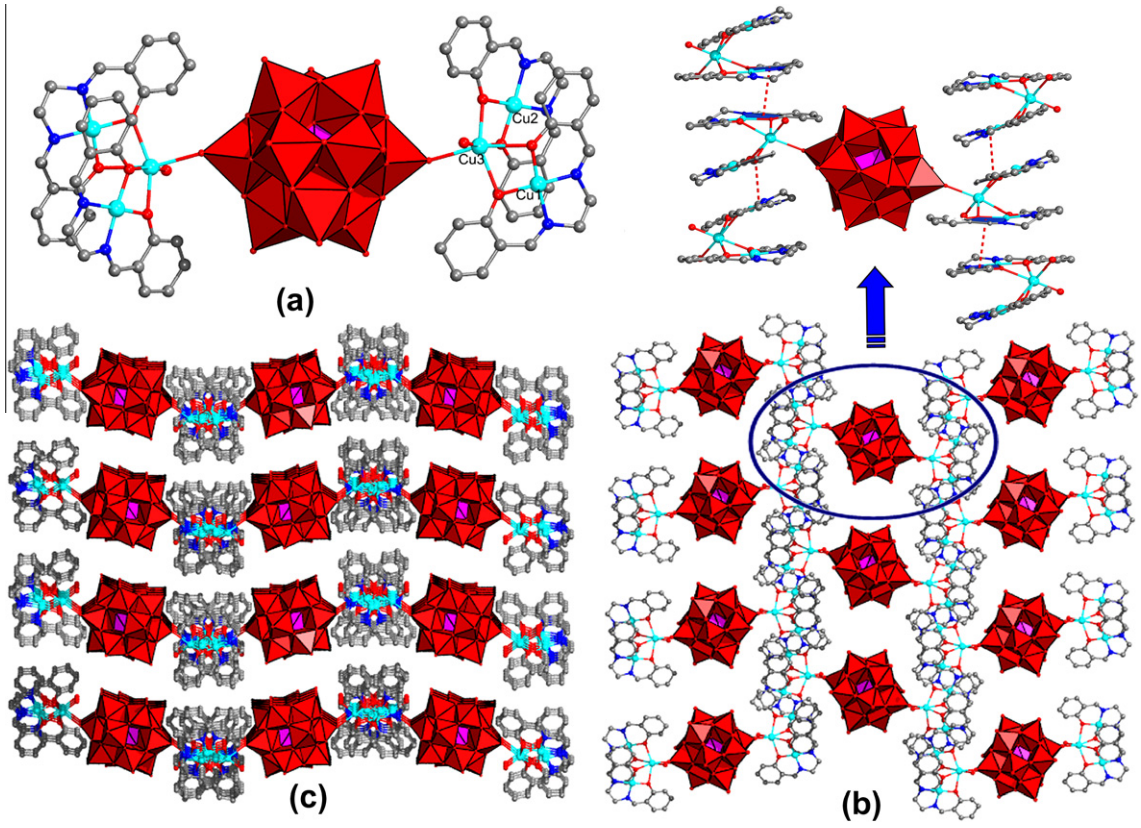

Fig. 5. (a) The molecular structure unit of compound **4**. (b) The two dimensional supramolecular layer of compound **4**. (c) The packing diagram of compound **4** along *a*-axis. All the hydrogen atoms have been omitted for clarity.

4. Photocatalysis experiments

It is well known that a series of POMs possess photocatalytic activities in the degradations of organic dyes [21]. Rhodamine-B (RhB) was selected as a representative to evaluate their catalytic activity. In the process of experiments, compounds **1**–**4** (1.0×10^{-5} mol) were respectively added into the 50 mL aqueous solution of RhB (2×10^{-5} mol L^{-1}). The solution was then exposed to UV irradiation from a 125 W Hg lamp, and always stirred during irradiation. At given time intervals, approximately 1 mL solvent was taken out and analyzed by UV–Visible spectroscopy.

In presence of compound **1**, the adsorption peak of RhB decreases speedily from 1.65 to 0.15 during 135 min of irradiation. With a rate of 5.67% per min for the decomposition of RhB solution, approximately 85% of RhB have been decomposed during the first 15 min, which indicates that compound **1** have a higher photocatalytic activity for the degradation of RhB. For compound **2**, the RhB degrades reposefully from 100% to 10.46% during 125 min. The degradation rate curve of **2** is nearly linear (inset in Fig. 6b), and the degradation rate is about 0.71% per min. For compound **3**, RhB degrades to 5.17% during 2 h and the degradation rate is 0.79% per min. For compound **4**, RhB degrades to 48.94% during 115 min and degradation rate is 0.44% per min. In addition, the metal–salens and POMs are added in the RhB solutions instead of compounds for contrast: Mn–salen and Cu–salen show no observable photocatalytic activity (Fig. S6 ESI†). At the beginning, the POMs show good catalytic activity, but later the concentration of RhB still maintain a high level and are not changed (Fig. S7 ESI†).

In summary, compound **1**–**3** showed better photocatalytic activity in the degradation of RhB in contrast with the polyanions used, which meant that using Mn–salen based POMs as photocatalyst, the degradation degree of RhB was higher than most of the POM system. As far as we know, the good photocatalytic activity of Mn–salen based hybrids may due to the synergetic effect between Mn–salen and POM. Meanwhile, the results of the control experiments indicated that the photocatalytic activity of compound **4** stemmed from the $SiW_{12}O_{40}^{4-}$ component. Consequently, the Mn–salen based hybrids possess better photocatalytic activity than POMs which may be used as a potential photocatalyst for the reduction of some organic dyes.

5. Electrochemical behaviors

The electrochemical behaviors of **1** and **2** modified carbon paste electrode (**1**-CPE and **2**-CPE) and their electrocatalytic reduction of nitrite have been investigated. Fig. S8 (ESI†) shows the cyclic voltammetric behavior of **1**-CPE in 1 M H_2SO_4 aqueous solution at different scan rates. The peak potentials change gradually following the scan rates from 50 to 300 mVs^{-1}. The cathodic peak potentials shift toward the negative direction, and the corresponding anodic peak potentials shift to the positive direction with increasing scan

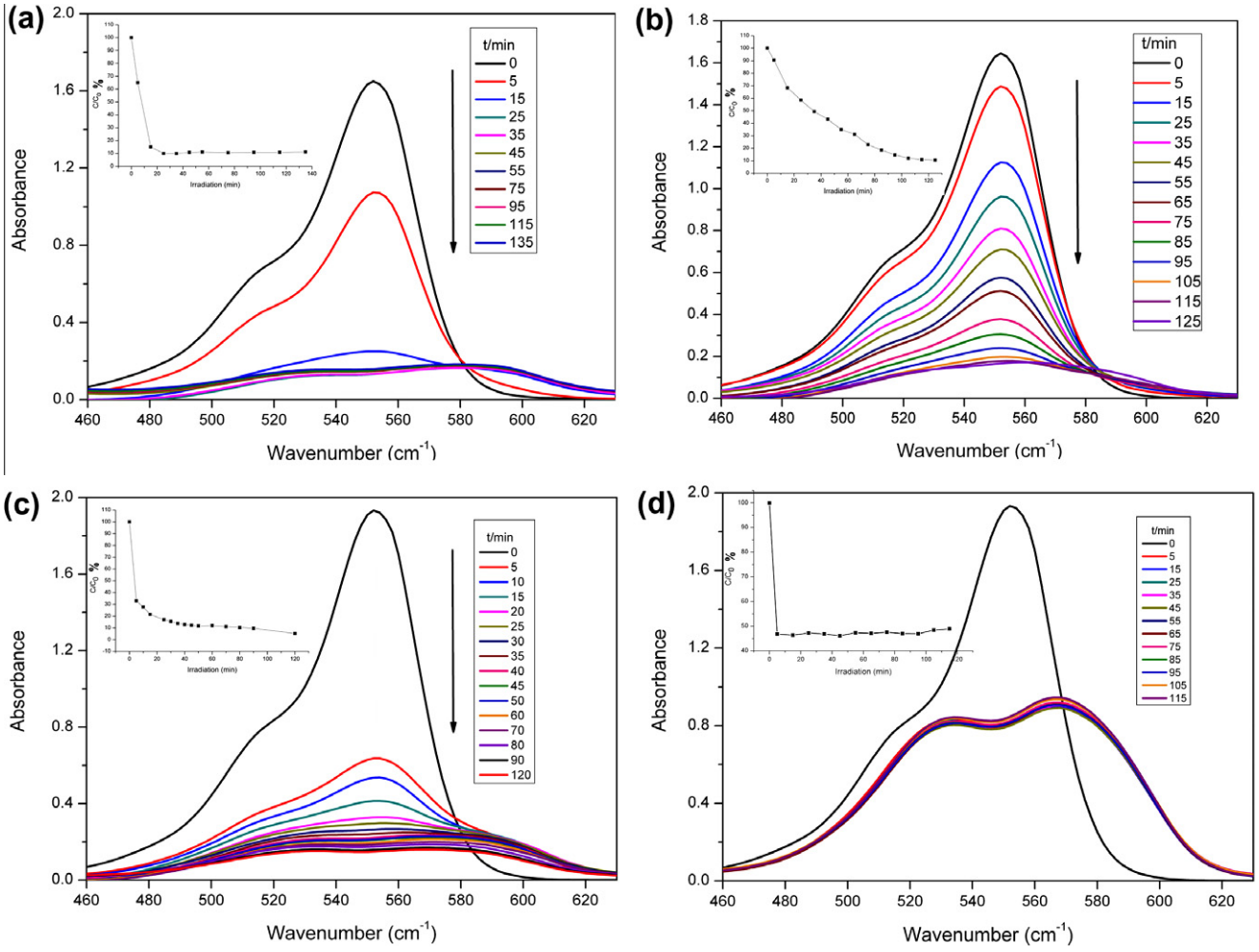

Fig. 6. Temporal UV–Visible absorption spectral changes observed for the 50 ml RhB solution as a function of irradiation time in the presence of 1×10^{-5} mol compound **1** (a); compound **2** (b); compound **3** (c); and compound **4** (d).

rates. The results verify that the redox ability of the polyanions can be maintained in the hybrid solids. It can be seen that two redox peaks appear at a potential range of –600 to 600 mV for compound **1** and –500 to 600 mV for compound **2**. Redox peaks I–I′ and II–II′ correspond to two-electron processes of W [22]. As shown in Fig. S8 (ESI†), **1**-CPE and **2**-CPE display good electrocatalytic activity toward the reduction of nitrite in 1 M H_2SO_4 containing $NaNO_2$. On addition of NO_2^-, the reduction peak currents increase and the corresponding oxidation peak currents decrease, which suggest that **1**-CPE and **2**-CPE have good electrocatalytic activity toward the reduction of nitrite.

6. TG analyses

In order to characterize the four compounds more fully in terms of their thermal stability, we investigated compounds **1**–**4** using TGA, as shown in Figs. S9–S12. The TG curve of **1** shows two weight loss processes. The first weight loss in the temperature range of 41–218 °C is might be attributed to the departure of coordination methanol molecules. The second weight loss starts at 330 °C and ends at about 764 °C. The ultimate remainder might be tungsten trioxide, silicon dioxide and manganese dioxide (found: 72.30%, calc: 72.23%). For compound **2**, it continuously decomposes and ends at 810 °C. The remainder products might be tungsten trioxide and manganese dioxide. (found: 78.73%, calc: 78.13%). Compound **3** shows two distinct weight loss steps. The first weight loss of in the temperature range of 42–312 °C, corresponds to the release of two $NH(CH_2CH_3)_3^+$ cations and two methanol molecules. The second weight loss in the temperature range of 316–743 °C can be assigned to the release of organic components. The TG curve of compound **4** suggests that in the range from 40 °C to approximately 290 °C, the lattice water molecules and coordination water molecules lose successively. On further heating, the remaining structure decomposes continuously and ends at about 680 °C. The ultimate remainder might be tungsten trioxide, silicon dioxide and copper oxide (found: 76.20%, calc: 76.17%).

7. Conclusions

In conclusion, we have successfully synthesized four compounds based on metal–salens and Keggin-type clusters. They are all characterized by X-ray single-crystal diffraction. These compounds display catalytic activity for photodegradation of RhB under UV irradiation and chemically bulk-modified carbon paste electrodes (**1**-CPE and **2**-CPE) exhibit good electrocatalytic activity toward the reduction of nitrite. It is expected to design and synthesize novel multifunctional hybrid POMs based on metal–salens, and more investigation is on going in our group.

Acknowledgements

This work was financially supported by the NNSF of China (Nos. 21001022 and 21171033), The National Grand Fundamental Research 973 Program of China (2010CB635114), Program for New Century Excellent Talents in Chinese University (NCET-10-0282), PhD Station Foundation of Ministry of Education (20100043110003), The Foundation for Author of National Excellent Doctoral Dissertation of PR China (FANEDD) (No. 201022), The Science and Technology Development Planning of Jilin Province (Nos. 201001169 and 20100182), The Fundamental Research Funds for the Central Universities (Nos. 09QNJJ018, 09ZDQD003, and 10CXTD001), and The Fundamental Research Funds for the Central Universities (11SSXT130).

Appendix A. Supplementary material

CCDC 831006–831009; contains the supplementary crystallographic data for this paper. These data can be obtained free of charge from The Cambridge Crystallographic Data Centre via www.ccdc.cam.ac.uk/data_request/cif. Supplementary data associated with this article can be found, in the online version, at http://dx.doi.org/10.1016/j.ica.2012.04.011.

References

[1] M.V. Vasylyev, R. Neumann, J. Am. Chem. Soc. 126 (2004) 884.
[2] T. Yamase, K. Fukaya, H. Nojiri, Y. Ohshima, Inorg. Chem. 45 (2006) 7698.
[3] (a) C. Sterb, D.L. Long, L. Cronin, CrystEngComm 8 (2006) 629;
(b) Y. Qi, E. Wang, J. Li, Y. Li, J. Solid State Chem. 182 (2009) 2640;
(c) C. Streb, C. Ritchie, D.L. Long, L. Cronin, Angew. Chem. Int. Ed. 46 (2007) 7579.
[4] G.A. Jeffrey, W. Saenger, Hydrogen Bonding in Biological Structures, Springer-Verlag, Berlin, 1991.
[5] K.D. Kreuer, S. Paddison, E. Spohr, M. Schuster, Chem. Rev. 104 (2004) 4637.
[6] R.P. Wayne, Chemistry of Atmospheres, Oxford University Press, New York, 1991.
[7] (a) R. Kumar, R.A. Christie, K.D. Jordan, J. Phys. Chem. B 113 (2009) 4111;
(b) G.E. Douberly, R.S. Walters, J. Cui, K.D. Jordan, M.A. Duncan, J. Phys. Chem. A 114 (2010) 4570;
(c) M. Park, I. Shin, N.J. Singh, K.S. Kim, J. Phys. Chem. A 111 (2007) 10692;
(d) O. Vendrell, F. Gatti, H. Meyer, Angew. Chem. Int. Ed. 46 (2007) 6918.
[8] (a) A. Müller, P.K. gerler, A.W.M. Dress, Coord. Chem. Rev. 222 (2001) 193;
(b) C. Streb, D.L. Long, L. Cronin, CrystEngComm 8 (2006) 629;
(c) C. Ritchie, E.M. Burkholder, D.L. Long, D. Adam, P. Kögerler, L. Cronin, Chem. Commun. (2007) 468.
[9] (a) T. Arumuganathan, A.S. Rao, S.K. Das, Cryst. Growth Des. 10 (2010) 4272;
(b) X. Liu, Y. Jia, Y. Zhang, R. Huang, Eur. J. Inorg. Chem. (2010) 4027;
(c) F. Yu, P.Q. Zheng, Y.X. Long, Y.P. Ren, X.J. Kong, L.S. Long, Y.Z. Yuan, R.B. Huang, L.S. Zheng, Eur. J. Inorg. Chem. (2010) 4526;
(d) Y.F. Song, D.L. Long, L. Cronin, Angew. Chem. Int. Ed. 46 (2007) 3900;
(e) C.P. Pradeep, F.Y. Li, C. Lydon, H.N. Miras, D.L. Long, L. Xu, L. Cronin, Chem. Eur. J. 17 (2011) 7472.
[10] J. Zhang, J. Hao, Y.G. Wei, F.P. Xiao, P.C. Yin, L.S. Wang, J. Am. Chem. Soc. 132 (2010) 14.
[11] H. Miyasaka, A. Saitoh, S. Abe, Coord. Chem. Rev. 251 (2007) 2622.
[12] (a) I. Bar-Nahum, A.M. Khenkin, R. Neumann, J. Am. Chem. Soc. 126 (2004) 10236;
(b) I. Bar-Nahum, R. Neumann, Chem. Commun. (2003) 2690;
(c) I. Bar-Nahum, H. Cohen, R. Neumann, Inorg. Chem. 42 (2003) 3677;
(d) V. Mirkhani, M. Moghadam, S. Tangestaninejad, I. Mohammadpoor-Baltork, N. Rasouli, Catal. Commun. 9 (2008) 2171.
[13] (a) Q. Wu, Y.G. Li, Y.H. Wang, R. Clérac, Y. Lu, E.B. Wang, Chem. Commun. (2009) 5743;
(b) Q. Wu, W.L. Chen, D. Liu, C. Liang, Y.G. Li, S.W. Lin, E.B. Wang, Dalton Trans. 40 (2011) 56;
(c) X. Meng, H.N. Wang, G.S. Yang, S. Wang, X.L. Wang, K.Z. Shao, Z.M. Su, Inorg. Chem. Commun. 14 (2011) 1418;
(d) X. Meng, C. Qin, X.L. Wang, Z.M. Su, B. Li, Q.H. Yang, Dalton Trans. 40 (2011) 9964.
[14] (a) H. Miyasaka, R. Clérac, T. Ishii, H.C. Chang, S. Kitagawa, M. Yamashita, Dalton Trans. (2002) 1528;
(b) H.L. Shyu, H.H. Wei, Y. Wang, Inorg. Chim. Acta 290 (1999) 8;
(c) J.M. Epstein, B.N. Figgis, A.H. White, A.C. Willis, Dalton Trans. (1974) 1954.
[15] X.L. Wang, C. Qin, E.B. Wang, Z.M. Su, Y.G. Li, L. Xu, Angew. Chem. Int. Ed. 45 (2006) 7411.
[16] G.M. Sheldrick, SHELXS-97, Program for X-ray Crystal Structure Solution, University of Göttingen, Göttingen, Germany, 1997.
[17] G.M. Sheldrick, SHELXL-97, Program for X-ray Crystal Structure Refinement, University of Göttingen, Göttingen, Germany, 1997.
[18] L.J. Farrugia, WINGX, A Windows Program for Crystal Structure Analysis, University of Glasgow, Glasgow, UK, 1988.
[19] I.D. Brown, D. Altermatt, Acta Crystallogr. B B41 (1985) 244.
[20] (a) L. Yuan, C. Qin, X.L. Wang, E.B. Wang, S. Chang, Eur. J. Inorg. Chem. (2008) 4936;
(b) P.P. Zhang, J. Peng, J.Q. Sha, A.X. Tian, H.J. Pang, Y. Chen, M. Zhu, CrystEngComm 11 (2009) 902;
(c) Z.G. Han, Y.Z. Gao, X.L. Zhai, J. Peng, A.X. Tian, Y.L. Zhao, C.W. Hu, Cryst. Growth Des. 9 (2009) 1225.
[21] (a) W.L. Chen, B.W. Chen, H.Q. Tan, Y.G. Li, Y.H. Wang, B. Wang, J. Solid State Chem. 183 (2010) 310;
(b) Y. Hu, F. Luo, F.F. Dong, Chem. Commun. 47 (2011) 761.
[22] (a) H.Y. Liu, H. Wu, J. Yang, Y.Y. Liu, J.F. Ma, H.Y. Bai, Cryst. Growth Des. 11 (2011) 1786;
(b) H. Jin, C. Qin, Y.G. Li, E.B. Wang, Inorg. Chem. Commun. 9 (2006) 482;
(c) M. Sadakane, E. Steckhan, Chem. Rev. 98 (1998) 219.